International Symposium
On Turbulence and Shear Flow
Phenomena (TSFP-9)
June 30 - July 3, 2015 *Melbourne, Australia*

TURBULENT MIXING IN CROSS SHEARED STRATIFIED FLOW

Y. Xiao, W. Lin, J. McCormack, Y. He
College of Sccience, Technology and Engineering
James Cook University
Townsville, QLD 4811, Austriala
email: yuan.xiao@my.jcu.edu.au
email: wenxian.lin@jcu.edu.au
email: jessie.mccormack@my.jcu.edu.au
email: yinghe.he@jcu.edu.au

S. W. Armfield, M. P. Kirkpatrick
School of Aerospace, Mechanical and Mechatronic Engineering
The University of Sydney
NSW 2006, Australia
email: steven.armfield@sydney.edu.au
email: michael.kirkpatrick@sydney.edu.au

ABSTRACT

Cross sheared stratified (CSS) flow, in which the horizontal streamwise and spanwise basic sheared flow components interact with each other in a stratified environment, are studied with direct numerical simulation. The cross shear ratio ξ, defined as $\xi = \Delta v_0/\Delta u_0$ where Δu_0 and Δv_0 are the respective velocity changes across the sheared/stratified layer in the streamwise and spanwise directions, is introduced for CSS flow. The coherent structures of CSS flow are examined for $\xi = 0 \sim 1$ and $Ri = 0.01 \sim 0.2$, where Ri is the bulk Richardson number. It is found that in a weakly stratified environment with $Ri = 0.01$, a significant increase of the magnitude of the mixedness thickness δ_m is observed from its time series for CSS flow compared to that for parallel sheared stratified flow. Three CSS instability modes, *i.e.* , a 'streamwise dominant' mode, a 'balanced' mode and a 'spanwise dominant' mode, are identified, which differ from each other with different interaction behaviors between the spanwise 'eddy wrap' structures and the classic streamwise 'cat eye' eddies of the Kelvin-Helmholtz instability. The results also show that in a strongly stratified environment with Ri=0.1-0.2, the eddy-featured coherent structures progressively decay into the wave-like structures, and the normalized mixedness thickness $\delta_\theta/\delta_{\theta,Ri=0.01}$ is found to decrease as an exponential function of increasing Ri at the turbulence stage.

INTRODUCTION

As a representative of geographical flows that occur inherently in stratified environments, the sheared stratified flows prevail in meso-scale geographical flows (e.g. , planetary or oceanic boundary layers), large scale stream flows (e.g. , rivers and estuaries), large water bodies (e.g. , reservoirs and lakes), and engineering applications (e.g. , mixing control in solar ponds and methane gas mixing in mine shafts). The understanding of mixing in sheared stratified flow also informs the design, control and safety of the mixing facilities in the chemical and pharmaceutical industries and other industrial areas. So far, the majority of the studies on sheared stratified flow have focussed on parallel sheared stratified (PSS) flow, whose basic flow velocity components in the Cartesian coordinates satisfy $V \ll U$, where U and V are the streamwise and spanwise components of the basic flow velocity in the x and y direction, respectively. However, in geographical and engineering scenarios with large horizontal extent, the magnitude of the spanwise velocity V is usually comparable to the streamwise counterpart U, resulting in cross sheared stratified (CSS) flow where comparable U and V coexist. Therefore, an additional control parameter, called the 'velocity shear ratio', is introduced for CSS flow to represent the relative magnitude of the spanwise velocity to the streamwise velocity and is defined as $\xi = \Delta v_0/\Delta u_0$, where Δu_0 and Δv_0 are the velocity changes across the sheared/stratified layer in the streamwise and spanwise directions respectively in the Cartesian coordinates.

The studies on the CSS flow are scarce. Atsavapranee & Gharib (1997) observed experimentally that the spanwise eddy structures have similar appearances to the streamwise Kelvin-Helmholtz 'cat eye' eddy structures through introducing the spanwise cross shear by tilting their water tank after the establishment of the streamwise structures, whereas Lin *et al.* (2000) reproduced numerically the spanwise eddies in a CSS flow that are similar to those observed by Atsavapranee & Gharib (1997). Both studies found that the mixing effect of CSS flow, in terms of the 'mixedness', is significantly increased when compared to PSS flow at the same conditions. Recently, a linear stability analysis by Xiao *et al.* (2014) on CSS flow suggests that the temporal growth rate of the unstable modes in CSS flow is much faster than thar in PSS flow.

In this paper, direct numerical simulation (DNS) is used to examine the effect of ξ and the bulk Richardson

number *Ri*, which will be defined in the next section, on the dynamics and mixing of CSS flow. The coherent structures of the CSS flow will be described using the concentration and vorticity contour plots and the mixing effect will be investigated in terms of the mixedness thickness.

METHODOLOGY

The governing equations for DNS are the continuity, Navier-Stokes, and density equations for incompressible flows with the Boussinesq approximation, which are written in the Cartesian coordinates (x, y and z) as follow:

$$\nabla \cdot \mathbf{u} = \mathbf{0} \tag{1}$$

$$\frac{\partial \mathbf{u}}{\partial t} + \mathbf{u} \cdot \nabla \mathbf{u} = -\nabla \frac{p}{\bar{\rho}} + g \frac{\rho - \bar{\rho}}{\bar{\rho}} \vec{k} + \nu \nabla^2 \mathbf{u} \tag{2}$$

$$\frac{\partial \rho}{\partial t} + \mathbf{u} \cdot \nabla \rho = \kappa \nabla^2 \rho \tag{3}$$

where $\mathbf{u}$ is the dimensional velocity vector, whose components in the x, y, z directions are u, v, w, t is time, p is pressure, ρ is density, ν and κ are the kinematic viscosity and thermal diffusivity of fluid, g is the gravitational acceleration, and $\bar{\rho}$ is a reference density with a value of 1027 kg/m^3. In the DNS, $\nu = 9.95 \times 10^{-7}$ m^2/s is used.

The differential operator ∇ is $\nabla = (\partial/\partial x)\vec{i} + (\partial/\partial y)\vec{j} + (\partial/\partial z)\vec{k}$, where $\vec{i}$, $\vec{j}$ and $\vec{k}$ represent the unit vector in x, y and z directions. The Laplacian operator ∇^2 is $\nabla^2 = (\partial^2/\partial x^2)\vec{i} + (\partial^2/\partial y^2)\vec{j} + (\partial^2/\partial z^2)\vec{k}$. The following typical velocity and density profiles of free shear flow are set up as the initial basic flow state:

$$\phi_0 = \Delta\phi_0 tanh[\frac{2}{\delta_s}(z - \frac{1}{2}L_z)], \tag{4}$$

in which ϕ represents u, v, ρ, the subscript '0' indicates the initial value of the physical property, Δu_0 and $\Delta\rho_0$ are the velocity and density changes across the initial sheared/stratified layer which has the initial thickness of δ_s, and L_z is the vertical extent of the domain under consideration. ξ is the cross shear ratio which represents the relative magnitude of the cross shear stresses in the spanwise direction compared to that in the streamwise direction and is defined as,

$$\xi = \frac{\Delta v_0}{\Delta u_0}.$$

To promote the coherent structures more efficiently, the following perturbations are imposed on the initial conditions, (4), aiming to excite the primary and secondary instabilities,

$$\begin{aligned}\phi_{pri} = \; & -0.02\Delta u_0 cos(\frac{2\pi x}{L_x}) sech[\frac{2}{\delta_s}(z - \frac{1}{2}L_z)] \\ & \times tanh[\frac{2}{\delta_s}(z - \frac{1}{2}L_z)],\end{aligned} \tag{5}$$

$$\phi_{sec} = A_\phi \Delta u_0 \{1 - |tanh[\frac{2}{\delta_s}(z - \frac{1}{2}L_z)]|\} r_\phi(x, y, z), \tag{6}$$

where the subscripts *pri* and *sec* denote the perturbation quantities for exciting the primary and secondary instabilities, respectively, r_ϕ is a random number between -1 and 1, A_ϕ is the amplitude coefficient for the secondary instability perturbations. For u, v, and ρ, A_ϕ are selected as 0.1, 0.1, and 0.5, respectively. As predicted by Xiao *et al.* (2014), the primary instability mode in CSS flows is a stationary mode usually corresponding to vortex structures, and the velocity shear will therefore be the predominant source to excite the primary instability. Accordingly, '*pri*' perturbations are only imposed on the two basic velocity components u and v, not on ρ. The initial field of a quantity will be the sum of the background profile, the primary perturbation, plus the secondary perturbation if applicable.

The periodic boundary conditions are applied in the horizontal directions. At the top and bottom boundaries, the impermeable condition is set for w and the zero flux boundary conditions are set for u, v, and ρ.

A reliable numerical code, PUFFIN, developed by Kirkpatrick (2014)), one of the current authors, is used to perform the DNS. The governing equations (1)-(3) are discretized in space using a finite volume formulation on a uniform, staggered, Cartesian grid. The advection terms in both the momentum and scalar transport equations used a 4th-order central difference scheme, while all other spatial derivatives are discretised using a second-order central difference scheme. The second order Adams-Bashforth and Crank-Nicolson schemes are used for the time advancement. The CFL number criterion is used to make sure the simulation is stable, with the minimum and maximum limits of 0.3 and 0.4, respectively. The discretised momentum and scalar equations are solved by the Gauss-Seidel method. The pressure correction equation is solved by the BICGSTAB solver with a modified strongly implicit preconditioner. The code is parallelized using Message Passing Interface (MPI).

The dimensions of the computational domain are set based on the stability analysis results of Xiao *et al.* (2014). L_x is choosen as $L_x = (2\pi/\alpha)(\delta_s/2)$ which is the one wavelength of the instability mode, in which α is the wavenumber corresponding to the most unstable mode. α is selected as 1/3 based on the stability analysis of Xiao *et al.* (2014). L_y and L_z are set to be equal to L_x to prevent the boundary intervention when coherent structures in the CSS flow become more expansive at $\xi > 0.5$. δ_s is set as 0.1795 m. The number of cells in the x, y and z directions are set as $256 \times 256 \times 128$, which is sufficient to capture the necessary features of the primary coherent structures.

The dimensionless parameters dictating the stability of flow are the initial bulk Reynolds number, *Re*, the initial bulk Richardson number, *Ri*, and the Prandlt number, *Pr*, defined as follows,

$$Re = \frac{\Delta u_0 \delta_s}{\nu}, \quad Ri = \frac{g\Delta\rho_0\delta_s}{\bar{\rho}(\Delta u_0)^2}, \quad Pr = \frac{\nu}{\kappa}.$$

As this study aims to investigate the primary coherent structures of CSS flow, *Re* is therefore selected as 1200, in the common range ($1000 \sim 2000$) for laboratory flows. $Pr = 1$ is used for all simulations. *Ri* will vary from 0.01 to 0.2 and ξ will vary from 0 to 1.

RESULTS

Coherent Structures

The typical evolution history of CSS flow structures leading to turbulence is demonstrated in figure 1, where the three-dimensional plots of the concentration c at four representative moments of the CSS flow instability evolution obtained by DNS are shown for the $\xi = 0.5$ case at $Ri = 0.01$. c is defined as:

$$c = \frac{\rho - \rho_1}{\rho_2 - \rho_1} \tag{7}$$

where ρ is the local density, $\rho_1 (= \bar{\rho} - 0.5\Delta\rho_0)$ and $\rho_2 (= \bar{\rho} + 0.5\Delta\rho_0)$ are the initial densities at the top and bottom boundaries. During the primary instability stage, when $t = 1000$ s as shown in figure 1(a), three spanwise eddies are observed. It seems that the bodies of spanwise eddies, especially the largest one close to the $y = 0$ plane, not only extend across the computational domain, but also wrap over the developing body of the 'cat eye' eddy. Therefore, unique spanwise 'eddy wrap' coherent structures are the prominent features of the CSS flow instability. Furthermore, the spanwise 'eddy wrap' and the streamwise 'cat eye' eddy structures continue to grow as shown in figure 1(b), followed subsequently by the commencement of the decay of the 'cat eye' eddy structures at about t =1600 s while the weaker spanwise eddies still expand as shown in figure 1(c). At t =2000 s, as shown in figure 1(d), the entire coherent structure collapses and a chaotic turbulent flow state appears.

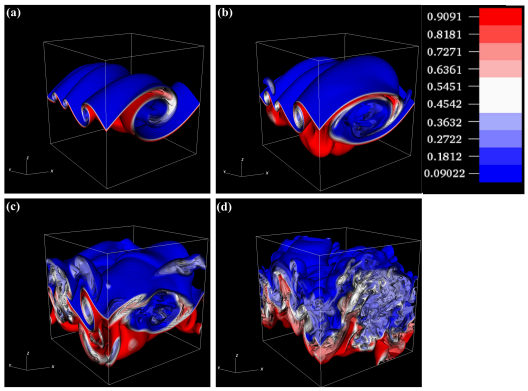

Figure 1. Contours of concentration c for the CSS flow instability in the $\xi = 0.5$ and $Ri = 0.01$ case: (a) the primary eddy wrap structure at $t = 1000$ s; (b) the collapse of the streamwise eddy and the growth of the spanwise eddy at $t = 1380$ s; (c) the collapse of the streamwise eddies and the entire coherent structure at $t = 1600$ s; and (d) the decay into turbulence at $t = 2000$ s.

When ξ changes, the evolution of the CSS flow structures basically follows in a similar fashion to that shown in figure 1. However, different appearances of the coherent structures are observed for different ξ values during the primary and secondary instability stages as shown in figure 2. The different coherent structures at different ξ values can be categorized as three types; a 'streamwise dominant mode'

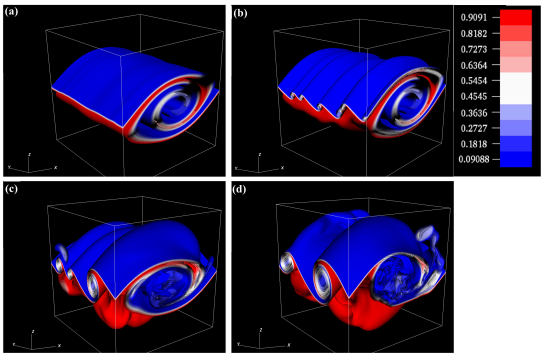

Figure 2. Contours of concentration c of the CSS flow at $Ri = 0.01$ with (a) the 'KH' mode for PSS flow with $\xi = 0.0$ at $t = 1380$ s, (b) the 'streamwise dominant' mode for CSS flow with $\xi = 0.2$ at $t = 1200$ s, (c) the 'balanced mode' for CSS flow with $\xi = 0.5$ at $t = 1380$ s, and (d) the 'spanwise dominant mode' for CSS flow with $\xi = 0.8$ at $t = 1200$ s.

with $\xi = 0.1 - 0.3$, a 'balance mode' with $\xi = 0.4 - 0.6$, and a 'spanwise dominant mode' with $\xi = 0.7 - 1.0$. The typical coherent structures for these three different modes are exhibited in figure 2(b) to figure 2(d), respectively. Also included in the figure is the typical 'cat eye' eddy structures for the 'KH' mode for PSS flow with $\xi = 0.0$ for comparison, as shown in figure 2(a). For the 'KH' mode, there is no overturning in the spanwise direction. As a weak cross shear with $\xi = 0.2$ is introduced, as shown in figure 2(b), several small spanwise 'eddy spots' are observed at the braid region of the streamwise 'cat eye' eddy. As ξ is further increaset to 0.5, the spanwise 'eddy spots' evolve into a 'eddy wrap' as shown in figure 2(c), where the 'cat eye' features become ambiguous at the center of the streawmwise eddy structures. At $\xi = 0.8$, as shown in figure 2(d), the enlarging spanwise 'eddy wrap' structure seems to suppress the streamwise 'cat eye' and lead to an internal collapse of the streamwise eddy structure from its center.

If the background stratification becomes stronger as Ri increases, the coherent structures observed in the weakly stratified environment as shown in figure 1 will more or less be suppressed, as demonstrated in figure 3 which shows the different primary coherent structures of CSS flow at different Ri values but with a fixed $\xi = 0.5$. When Ri is increased from 0.01 to 0.05, as shown in figure 3(a) and figure 3(b), both the streamwise 'cat eye' eddy and the spanwise 'eddy wrap' eddy structures seem to be compressed towards the eddy core, as the size of the coherent eddy structures diminishes while the concentrations c at the eddy cores increase from $0.01 \sim 0.18$ as shown by blue contour to $0.45 \sim 0.55$ as shown by white contour. At $Ri = 0.15$, as shown in figure 3(c), both the streamwise and spanwise eddy structures degrade into overturning structures, whose sizes further decrease when compared to the $Ri = 0.05$ case. At $Ri = 0.2$, as shown in figure 3(d), the spanwise overturning structures further decay into wave-featured structures due to a stronger background stratification, while on the other hand the spanwise overturning seems to reversely grow stronger, suggesting a complicated mechanisms in strongly stratified environments.

As coherent structures in the CSS flow display strong eddy features, it is very helpful to further examine the vorticity contour plots corresponding to the c contour plots.

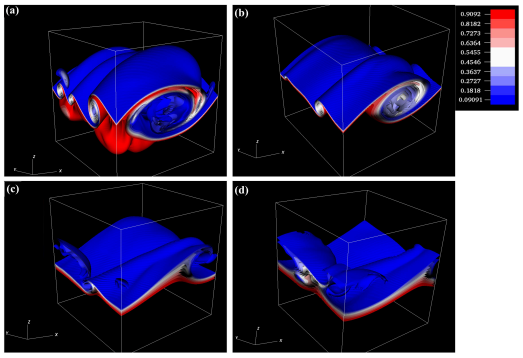

Figure 3. Contours of concentration c of CSS flow at ξ=0.5 with (a) Ri =0.01 at t =1380 s, (b) Ri =0.05 at t =1500 s, (c) Ri =0.15 at t =1250 s, and (d) Ri =0.20 at t =1500 s.

Figure 4 shows the slice plot of the streamwise vorticity contours at Ri =0.01 with different ξ values. The streamwise vorticity is defined as:

$$\omega_x = \frac{\partial w}{\partial y} - \frac{\partial v}{\partial z}. \tag{8}$$

For the KH instability case (at $\xi = 0$), this slice plane is the vertical central plane at $y = 0.5L_y$, and for the CSS flow instability cases, it is the vertical slice plane determined by the initial point (0, y_i, 0) and the direction vector (0.99$\vec{i}$, 0.12$\vec{j}$, 0.0$\vec{k}$), rather than in the x direction, due to the slight misalignment of the symmetry axis of the spanwise eddy wrap structure with the x direction. For $\xi = 0.2$ and 0.5, $y_i = 0.25L_y$, and for $\xi = 0.8$, $y_i = 0.3125L_y$.

For the 'KH' mode as shown in figure 4(a), the positive and negative ω_x regions alternatively fill in the 'cat eye' eddy core area, while in the braid region only positive ω_x exists. As cross shear is introduced, negative ω_x representing the spanwise vorticity tube appears in the braid regions as well. At $\xi = 0.2$, as shown in figure 4(b), the negative ω_x in the braid regions is still very weak, which corresponds to the weak appearances of spanwise eddies shown in figure 2(b). At ξ =0.5, as shown in figure 4(c), the significant spanwise 'eddy wrap' structures represented by large negative ω_x regions surround the central 'cat eye' eddy core, where positive ω_x dominates. Compared to the 'KH' mode and the 'streamwise dominant' mode, the sizes of the central 'cat eye' eddies in the ω_x plot are smaller, indicating that the expanding spanwise 'eddy wrap' structures largely suppress the streamwise eddy structures. A complete domination of the spanwise 'eddy wrap' occurs for the 'spanwise dominant mode' as shown in figure 4(d), where only a small positive ω_x spot survives in the center. The significantly degrading 'cat eye' structures shown in figure 4(d) supports the observations from figure 2(d) that the streamwise eddy structures collapse from its core.

The influence of Ri is also examined with the ω_x plots as shown in figure 5 for $\xi = 0.5$ and four Ri values which are the same as those in figure 3. As Ri increases to 0.05, the spanwise 'eddy wrap' structures reduce to thin and extended eddy tubes, as shown in figure 5(b). The streamwise 'cat eye' eddies at the center of the domain are compressed as a result of the enhanced background stratification so that a more evident 'cat eye' shape is observed when compared

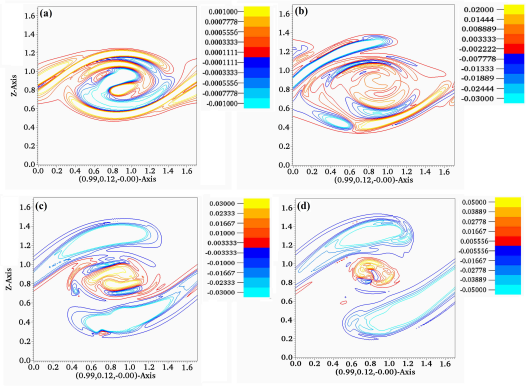

Figure 4. Contours of ω_x in a vertical slice plane for CSS flow in a weakly stratified environment at $Ri = 0.01$ with (a) $\xi = 0.0$ at $t = 1600$ s, (b) $\xi = 0.2$ at $t = 1500$ s, (c) $\xi = 0.5$ at $t = 1200$ s, and (d) $\xi = 0.8$ at $t = 1050$ s. The cold(hot) color denotes a negative(positive) ω_x.

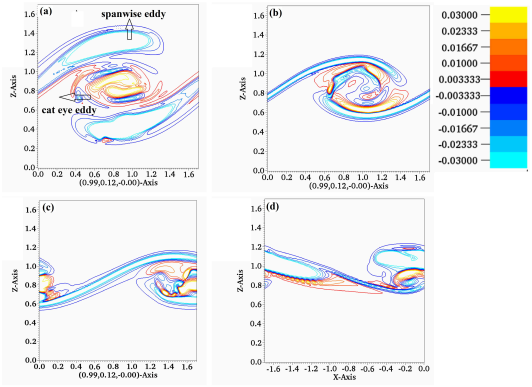

Figure 5. Contours of ω_x in a vertical slice plane for CSS flow with $\xi = 0.5$ and at (a) Ri=0.01 at $t = 1200$ s, (b) Ri=0.05 at $t = 1500$ s, (c) Ri=0.15 at $t = 1250$ s, and (d) Ri=0.2 at $t = 1500$ s. The cold(hot) color denotes a negative(positive) ω_x.

to that in figure 5(a). As Ri is further increased, the entire coherent structures start to propagate across the periodic streamwise boundaries. When Ri =0.15, the size of streamwise 'cat' eye eddy further decreases as shown in figure 5(c) and at Ri=0.20 the eddy structures are totally replaced by the propagating wave-featured structures seen in figure 5(d), where the spanwise wave structures grow larger compared to a small spanwise overturning structure in figure 5(c). The growing spanwise wave structures suggest that more complicated mechanisms might be involved in CSS flow with large background stratifications.

Mixedness

The mixing effect in CSS flow can be quantified by a quantity called mixedness, $M(z,t)$, introduced by Konrad (1976). $M(z,t)$ represents the ratio between the densities with and without fluctuations. The mixedness thickness, δ_θ,

is obtained by the integration of $M(z,t)$, *i.e.*,

$$\delta_\theta = \int_0^{L_z} M(z,t)dz. \tag{9}$$

Figure 6 presents the time series of δ_θ for ξ varying over the range $0 \le \xi \le 1.0$. For each ξ value, three development stages are observed for δ_θ; a short slow growth stage, a rapid growth stage and finally an asymptotic stage. In the slow growth stage, δ_θ for all ξ values almost overlap. In the rapid growth stage, the magnitude of δ_θ generally increases significantly with increasing ξ, indicating effective improvements in mixing. Thus, during the rapid growth stage, the CSS flow instability is far more effective in terms of the mixing effect than the traditional KH instability. This is in line with the experimental observations by Atsavapranee & Gharib (1997) and Lin *et al.* (2000). Nonetheless, it is observed that the CSS flow has no obvious advantages in terms of the mixing effect at the asymptotic stage, as there is little difference between the values of δ_θ for $\xi \ge 0.4$ cases.

When δ_θ is normalized by $\delta_{\theta,\xi=0}$, two peaks are clearly shown in figure 7 and are marked as the 'first peak' and the 'second peak', which indicate the developed primary instability and the saturation of the coherent structures respectively. Two peaks found in the time series of $\delta_\theta/\delta_{\theta,\xi=0}$ at different ξ reflect the results of the normalization factor $\delta_{\theta,\xi=0}$, in which the primary instability and the secondary instability are distinct from each other, as seen in figure 6. Similar to figure 6, asymptotic stages are found in figure 7 where at different ξ values δ_θ is not so significant compared to those at the primary(second) instability stage as marked by 'first(second) peak'.

With appearances of two peaks, the differences among three CSS instability modes are more obvious in the time series of $\delta_\theta/\delta_{\theta,\xi=0}$. For the 'streamwise dominant' mode with $\xi = 0.1-0.3$, the second peak is significantly higher than the first peak, indicating that the mixing process is stronger at the saturation stage. This is physically reasonable because in the 'streamwise dominant' mode, the streamwise 'cat eye' eddy still dominates over the weak spanwise 'eddy wrap' structures, therefore the expansion of the KH eddy contributes more to the spanwise saturation process. In the 'balanced' mode with $\xi = 0.4-0.6$, the first peak catches up with the second, indicating that the primary and secondary instabilities achieve almost the same amount of mixing due to the gradually stronger spanwise eddy structures. In the 'spanwise dominant' mode, the first peak overtakes the second peak and becomes the dominant factor in the turbulence mixing. This is because the streamwise KH eddy is strongly suppressed by the spanwise eddy as shown in figure 2(d) and figure 4(d). It is noted that the time span from the first peak to the second peak is decreasing with increasing ξ, indicating faster transition to turbulence in the CSS flow with increasing ξ.

As Ri further increases, the evolution of δ_θ is modified by the increasing background stratification. Figure 8 shows the normalized δ_θ at Ri =0.15 with $0 \le \xi \le 1.0$. Compared to figure 6, only a single peak is found at about t =2500 s, when the saturation of the coherent structures commences before the turbulence stage. The disappearance of the first peak associated with the primary instability at $Ri = 0.15$ corresponds to the suppressed appearance of the primary coherent structures observed in figure 3(c).

To compare with the experimental results obtained by Atsavapranee & Gharib (1997) during the turbulence stage

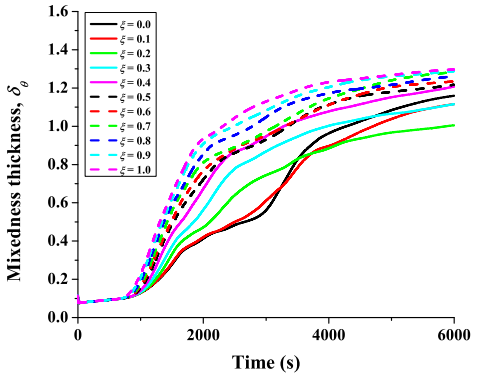

Figure 6. Time series of δ_θ at $Ri = 0.01$ with ξ varying over the range of $0 \le \xi \le 1.0$.

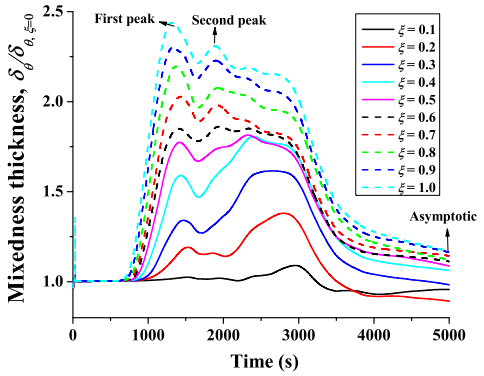

Figure 7. Time series of the normalized mixedness thickness $\delta_\theta/\delta_{\theta,\xi=0}$ at $Ri = 0.01$ with ξ varying over the range of $0 \le \xi \le 1.0$.

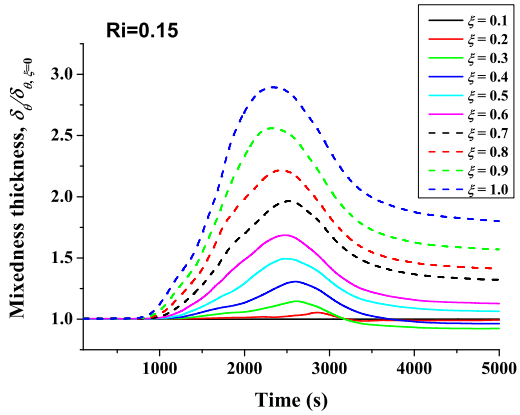

Figure 8. Time series of the normalized mixedness thickness $\delta_\theta/\delta_{\theta,\xi=0}$ at $Ri = 0.15$ with ξ varying over the range of $0 \le \xi \le 1.0$.

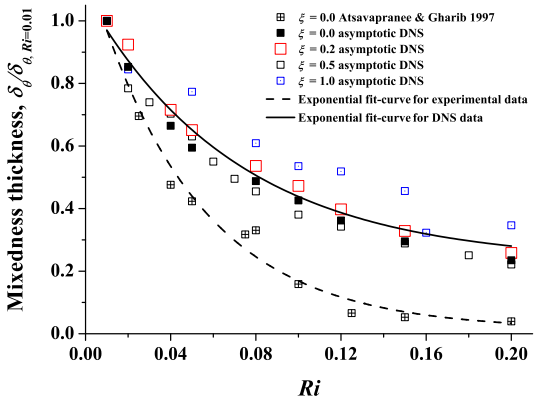

Figure 9. $\delta_\theta/\delta_{\theta,Ri=0.01}$ at the turbulence stage obtained experimentally by Atsavapranee & Gharib (1997) and numerically by the current study plotted against Ri.

(the asymptotic stage as shown in figure 6), δ_θ obtained in this numerical study and in the experimental study of Atsavapranee & Gharib (1997) are normalized by their corresponding values of δ_θ at Ri =0.01. The normalized $\delta_\theta/\delta_{\theta,Ri=0.01}$ are shown in figure 9, where the numerical results and the experimental results are represented by the void and solid points, respectively. The gaps between the experimental results and the DNS results are observed and are found to have further increases after approximately $Ri = 0.03$. Such increasing gaps are a result of the different length scale setup in Atsavapranee & Gharib (1997) and this study. In the current DNS simulation only a single wavelength of the unstable mode is used with periodic boundary conditions, while in the experiments of Atsavapranee & Gharib (1997) the water tank extends the length of several unstable mode units. Therefore the coupling between adjacent flow structures, such as pairing between two adjacent eddy structures, are unable to be produced in the current DNS study. Nevertheless, at small Ri ($Ri < 0.03$) where the length scales of unstable flow structures are larger due to less suppression from the stratification, the experimental results and the current DNS results correlate very well.

The following best-fit correlations between $\delta_\theta/\delta_{\theta,Ri=0}$ and Ri at the asymptotic stage are obtained,

$$\delta_\theta/\delta_{\theta,Ri=0.01} = 0.22874 + 0.85318\times(8.01364\times10^{-7})^{Ri} \quad (10)$$

for the DNS results and

$$\delta_\theta/\delta_{\theta,Ri=0.01} = 0.0131 + 1.16979\times(1.74621\times10^{-9})^{Ri} \quad (11)$$

for experimental results, as shown in figure 9. However, the data with $\xi = 1.0$ deviates considerably from the correlations, implying that a different dynamic mechanism occurs at high cross shear.

CONCLUSIONS

In this study, a cross shear ratio ξ is introduced in PSS flow to create a CSS flow configuration. The influence of the cross shear ratio ξ representing the relative contribution of the cross shear and the bulk Richardson number Ri representing the relative intensity of the background stratification with respect to the mainstream velocity shear is investigated numerically for the CSS flow over the ranges of $\xi = 0 \sim 1$ and $Ri = 0.01 \sim 0.2$. For the weakly stratified environment where the velocity shear dominates, three types of the CSS flow instability modes are found: the 'streamwise dominant' mode with $\xi = 0.1 \sim 0.3$, the 'balanced' mode with $\xi = 0.4 \sim 0.6$, and the 'spanwise dominant' mode with $\xi = 0.7 \sim 1.0$. They differ from each other with different interaction behaviors between the spanwise 'eddy wrap' structures and the classic streamwise 'cat eye' eddies of the KH instability. For stronger background stratifications with increased Ri values, the eddy-featured coherent structures are suppressed and ultimately downgraded to wave-like coherent structures.

The time series of the mixedness thickness δ_m for weakly stratified environments show significant increases of δ_m at the primary and secondary instability stages in CSS flow compared to PSS flow. After normalization of δ_m by δ_m at ξ =0 for PSS flow, two peaks appear in the times series of the normalized mixedness thickness $\delta_\theta/\delta_{\theta,\xi=0}$ as manifestations of primary and secondary instabilities. In the times series of $\delta_\theta/\delta_{\theta,\xi=0}$, the features of the three CSS flow instability modes are clearly identified by whether $\delta_\theta/\delta_{\theta,\xi=0}$ at the first peak (the primary instability stage) is more than, comparable to, or less than $\delta_\theta/\delta_{\theta,\xi=0}$ at the second peak (the secondary instability stage). Furthermore, as Ri increases up to 0.05, two peaks found in the time series of $\delta_\theta/\delta_{\theta,\xi=0}$ at $Ri = 0.01$ reduce to a single peak, which occurs at the time when the coherent structures saturate. Finally, it is also found that the normalized mixedness thickness $\delta_\theta/\delta_{\theta,Ri=0.01}$, which is normalized by δ_m at Ri =0.01, decreases as an exponential function of Ri at the turbulence stage.

ACKNOWLEDGEMENT

The support from the Australian Research Council is gratefully acknowledged. Y. Xiao also would like to thank James Cook University for the JCUPRS scholarship.

REFERENCES

Atsavapranee, P. & Gharib, M. 1997 Structures in stratified plane mixing layers and the effects of cross-shear. *Journal of Fluid Mechanics* **342**, 53–86.

Kirkpatrick, M. P. 2014 The puffin manual: An engineering and environmental fluid dynamics simulation model. Technical report. The Univ. of Sydney, Sydney.

Konrad, J. H. 1976 An experimental investigation of mixing in two-dimensional turbulent shear flows with applications to diffusion-limited chemical reactions. PhD thesis, California Institue of Technology, Pasadena, CA.

Lin, J., Shao, X. & Yu, Z. 2000 Numerical research on coherent structures in a mixing layer with cross-shear. *Acta Aeronautica et Astronautica Sinica* **20**, 13–20.

Xiao, Y., Lin, W., Armfield, S. W., Kirkpatrick, M. P. & He, Y. 2014 Hydrodynamic linear stability analysis on cross sheared stratified flows. In *Proceedings of 19th Australasian Fluid Mechanics Conference*. Melbourne, Australia.